

Origins of Stereoselectivities in Chiral Phosphoric Acid Catalyzed Allylboration and Propargylation of Aldehydes

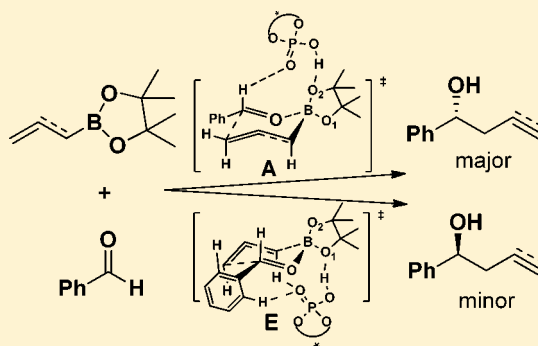
Hao Wang,[†] Pankaj Jain,[‡] Jon C. Antilla,[‡] and K. N. Houk^{*,†}

[†]Department of Chemistry and Biochemistry, University of California, Los Angeles, California 90095-1569, United States

[‡]Department of Chemistry, University of South Florida, 4202 East Fowler Avenue, Tampa, Florida 33620, United States

S Supporting Information

ABSTRACT: The chiral BINOL-phosphoric acid catalyzed allylboration and propargylation reactions are studied with density functional theory (B3LYP and B3LYP-D3). Two different models were recently proposed for these reactions by Goodman and our group, respectively. In Goodman's model for allylboration, the catalyst interacts with the boronate pseudoaxial oxygen. By contrast, our model for propargylations predicts that the catalyst interacts with the boronate pseudoequatorial oxygen. In both models, the phosphoric acid stabilizes the transition state by forming a strong hydrogen bond with the oxygen of the boronate and is oriented by a formyl hydrogen bond (Goodman model) and by other electrostatic attractions in our model. Both of these models have now been reinvestigated for both allylboration and propargylation. For the most effective catalyst for these reactions, the lowest energy transition state corresponds to Goodman's axial model, while the best transition state leading to the minor enantiomer involves the equatorial model. The high enantioselectivity observed with only the bulkiest catalyst arises from the steric interactions between the substrates and the bulky groups on the catalyst, and the resulting necessity for distortion of the catalyst in the disfavored transition state.



INTRODUCTION

Asymmetric allylboration of carbonyls are valuable methods in organic synthesis and occur with high enantioselectivity and diastereoselectivity.¹ The most common method for enantioselective allylboration involves chiral allylboron reagents.² However, the preparation of chiral allylboranes and allyl boronates often requires multiple steps and can be challenging. Enantioselective allylboration involving catalytic chiral Lewis acids³ or Brønsted acids⁴ have now been developed. In particular, chiral BINOL-phosphoric acids that have been employed in many other asymmetric reactions^{5,6} were recently demonstrated by Antilla to catalyze the enantioselective allylboration reaction between allylboronate **1** and benzaldehyde **2** (Figure 1).⁷ The homoallylic alcohol **3** was obtained in 99% yield and 93% ee with catalyst **PA1** bearing bulky 3,3'-substituents. For other aldehydes, including electron-donating aromatic aldehydes, electron-withdrawing aromatic aldehydes, and aliphatic aldehydes, the enantioselectivities vary from 73% to 99% ee. The asymmetric propargylation involving allenyl boronic acid pinacol ester **1'** and benzaldehyde **2** was efficiently catalyzed by **PA1** as well, which gave homopropargylic alcohol **3'** in high yield and ee.⁸ Catalysts where the Ar groups are less bulky gave much lower ee values.

Using computational methods, we recently proposed a model to explain the enantioselectivities in propargylations.⁸ In our model (Figure 2), the phosphoric acid establishes a H-bond with the pseudoequatorial oxygen of the boronate. The high

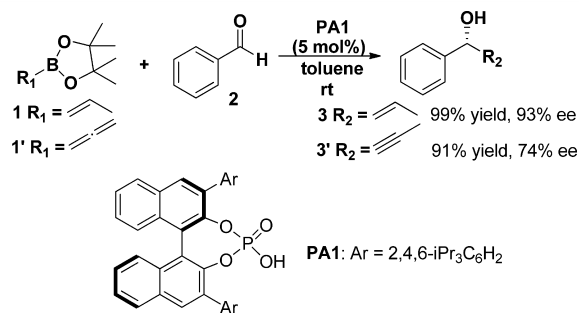


Figure 1. Chiral phosphoric acid catalyzed allylboration and propargylation of benzaldehyde.

enantioselectivities observed for **PA1** originate from the larger distortion of the catalyst in the disfavored TS, which is the result of avoiding steric interactions between the allenylboronate methyls and the bulky substituents in the catalyst. At almost the same time, Grayson, Pellegrinet, and Goodman published a computational study of allylboration reactions.⁹ In the Goodman et al. work, it was proposed that the hydroxyl group of BINOL phosphoric acid H-bonds to the pseudoaxial oxygen of the boronate, and the phosphoryl oxygen interacts with the aldehyde formyl hydrogen through electrostatic

Received: December 22, 2012

Published: January 8, 2013

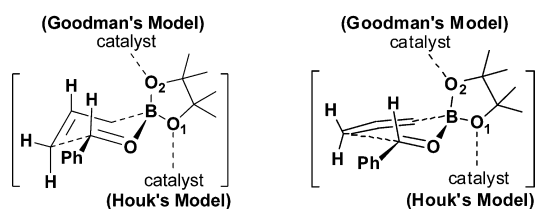


Figure 2. Two models for the chiral phosphoric acid catalyzed allylboration and propargylations of benzaldehyde.

interactions (Figure 2). Due to the large size of the real catalyst, Goodman used ONIOM calculations on the full catalyst PA1. The high enantioselectivities were rationalized from the unfavorable steric clash between the pinacol methyl groups and the large alkyl-substituted aromatic group of the catalyst. Despite the differences in the activation modes of the two models, steric effects or the resulting distortions of the catalyst are believed to determine the origins of the stereoselectivities in these reactions.

We have reinvestigated the chiral BINOL-phosphoric acid catalyzed allylboration and propargylation reactions using several levels of DFT calculations. In order to study the enantioselectivity of the catalysis, the two different models were evaluated. In addition, we used B3LYP-D3, which includes dispersion energies,¹⁰ to calculate the transition state energies, which may also be important to such systems. Using biphenol (BIPOL)-derived phosphoric acid as the model catalyst, we found that the two competing models are comparable in energy. The diastereomeric TSs involved in allylboration and propargylations for PA1 were located using fully DFT optimization, and the calculated energies by B3LYP and B3LYP-D3 indicated that both pathways were involved for these systems. Goodman's model with axial coordination has a lower energy for the *re*-face attack TS, which leads to the major enantiomeric product. However, in our calculations, for the *si*-face attack TS, our model is more stable than Goodman's model, which indicated that the minor enantiomeric TS comes from equatorial coordination of the catalyst.

RESULTS AND DISCUSSION

Investigation of the Reaction Mechanism. The allylboration reaction proceeds via a closed six-membered chairlike transition state.¹¹ There are three possible coordination positions for the catalyst hydroxyl group: the two boronate oxygens or the aldehyde oxygen (Figure 3). In Goodman's and our models, the phosphoric acid forms a hydrogen bond with the boronate oxygens: either the pseudoequatorial oxygen (path i: eq), or the pseudoaxial oxygen (path ii: ax). The other

plausible mechanistic pathway is the phosphoric acid forming a H-bond with the oxygen of the aldehyde (path iii).

In order to evaluate these different pathways, we first explored transition states where each of the oxygens was protonated. All calculations were performed with the Gaussian 09 package.¹² Geometries were fully optimized in the gas phase and characterized by frequency calculations using B3LYP functional and 6-31G* basis set. Free energies were calculated for each stationary point. The optimized chairlike transition state structure of the uncatalyzed reaction is shown in Figure 4, and the transition states for the three possible sites of protonation are shown in Figure 5 along with their relative Gibbs free energies.

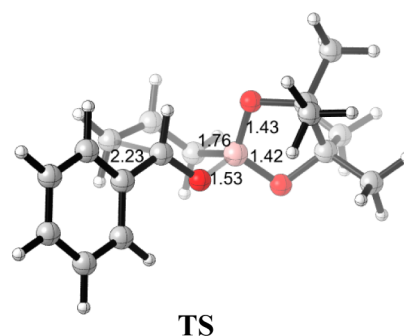


Figure 4. Optimized transition state of the uncatalyzed allylboration of benzaldehyde at the B3LYP/6-31G* level of theory.

As shown in Figure 5, the pathways involving protonation of boronate oxygens (TS1, 0.0 kcal/mol; TS2, +3.6 kcal/mol) are more favorable than TS3 (+4.3 kcal/mol), which involves protonation of the aldehyde oxygen. Protonation of a B–O increases the electrophilicity of the boronate and lowers the activation energy.¹³ This finding is in agreement with Hall's experimental observations¹⁴ and Fujimoto's theoretical studies¹⁵ of similar Lewis acid catalyzed allylboration reactions. Similarly, for propargylations, protonation of boronate oxygens accelerates more than protonation of aldehyde (See Supporting Information).

Model of the Phosphoric Acid Catalyzed Allylboration Reaction. The mechanistic studies reported above illustrate that activation of boronate oxygens are more favorable than activation of aldehyde oxygen. This phenomenon is also found in Goodman's model study calculations. In order to better understand the boronate activation pathways, catalyst PA without Ar substituents was then employed to study both paths i and ii in more detail. In order to reduce the computational cost, the biphenol (BIPOL)-derived phosphoric acid was initially used as the model instead of the BINOL-derived

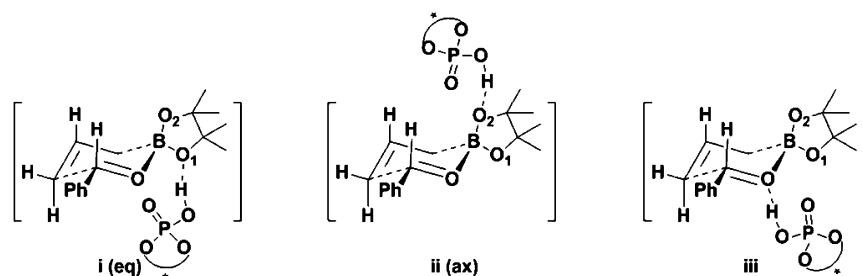


Figure 3. Three possible sites of coordination in the phosphoric acid catalyzed allylboration reaction.

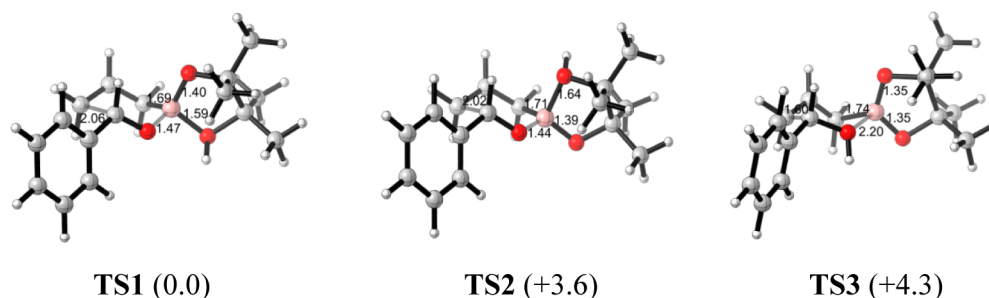


Figure 5. Optimized transition states of different mechanisms at the B3LYP/6-31G* level of theory. Bond lengths are given in Å. Relative free energies (kcal/mol) are shown in parentheses.

phosphoric acid. This kind of truncating has previously been justified by Yamanaka, Akiyama, and Goodman in their studies.⁶ Replacement of the binaphthyl backbone with a smaller biaryl does not significantly alter the geometry around the reaction center.

In both pathways i (eq) and ii (ax), the catalyst interacts with the allylboronate by a single hydrogen bond, and the orientation of the phosphate with respect to the substrate is not fixed. As a result, the remaining parts of the catalyst are conformationally flexible, and there are many possible diastereomeric transition state structures with different orientations of the catalyst. To explore all accessible conformations of the transition states, a conformational search was performed (see Supporting Information, Figure S1).

For pathway i, two low energy transition state structures, **TS4** and **TS4'**, were located for the phosphoric acid catalyzed allylboronation reaction (Figure 6a). In **TS4**, the lowest energy minimum for i, the phosphoryl oxygen was near the six-membered transition state; in **TS4'**, the phosphoryl oxygen is

away from the six-membered ring, but next to the boronate methyls. **TS4'** is 1.4 kcal/mol less stable than **TS4**. Since B3LYP may underestimate the aromatic and dispersion interactions in such systems, a method that is expected to treat such interactions more accurately was used to calculate the energy differences between different transition states as well. The energy difference between **TS4** and **TS4'** is calculated to be 2.0 kcal/mol with B3LYP-D3, which includes a dispersion energy correction. For pathway ii, involving H-bonds to the pseudoaxial boronate oxygen, two different diastereomeric transition state conformers, **TS5** and **TS5'**, were also found (Figure 6b). **TS5**, in which the phosphoryl oxygen is situated over the six-membered ring TS, was more energetically favorable than **TS5'** by 3.0 kcal/mol. B3LYP-D3 calculation gave an energy difference of 3.5 kcal/mol between **TS5** and **TS5'**. This order of stability between **TS5** and **TS5'** was also observed by Goodman et al.⁹

In order to study the origin of the energy differences between the different transition state conformers, electrostatic potentials were computed. They are shown for the uncatalyzed reaction transition state **TS** in Figure 7. The formyl H, allyl H's and

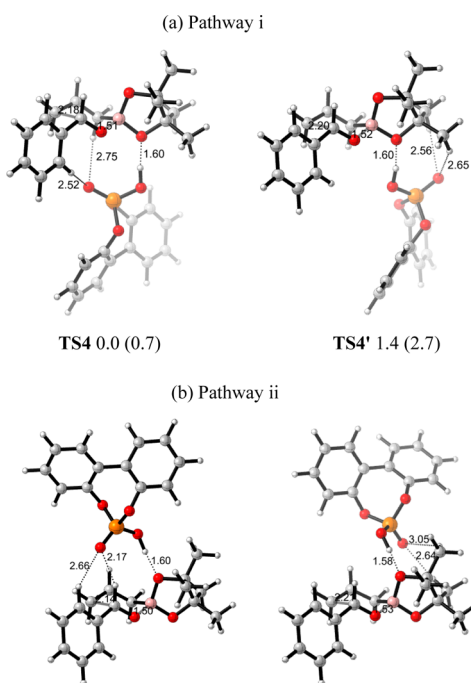


Figure 6. Optimized transition state structures of (a) **TS4**, **TS4'** in pathway i (eq) and (b) **TS5**, **TS5'** in pathway ii (ax) at the B3LYP/6-31G* level of theory. Bond lengths are given in Å. Values next to each structure are energies relative to **TS4** in kcal/mol. Values in parentheses are energies relative to **TS5** calculated by B3LYP-D3.

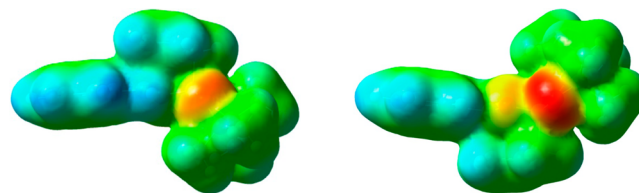


Figure 7. Top and bottom view of electrostatic potential of **TS** from Figure 4. Red, negative ESP; blue, positive ESP; green, neutral.

phenyl H's are more positive than the H's on boronate methyls. This indicates that there can be stabilizing electrostatic attractions between the phosphoryl oxygen and those positive H's. The stabilized interactions between electronegative parts of catalysts and the formyl H has been proposed by Corey before,¹⁶ as well as in Goodman's model. Here, **TS4** was more stable than **TS4'** and **TS5** was more stable than **TS5'**. The extra stabilization of **TS4** and **TS5** comparing to **TS4'** and **TS5'** came from the extra attractive P=O...H-C interactions, either with the aldehyde H in **TS5** or the phenyl and allyl H's in **TS4**.

By comparing the most stable TSs in two pathways, **TS4** is calculated to be 0.2 kcal/mol more stable than **TS5** by B3LYP, but 0.7 kcal/mol less stable than **TS5** using B3LYP-D3. In the Goodman et al. work, when buta-1,3-diene-1,4- diol-phosphoric acid, which contains no aromatic rings, was used as the model catalyst, the two competing pathways are differentiated by 2.2 kcal/mol. In our studies, the model catalyst (biphenol-derived

phosphoric acid) resembles more the real catalysts in the experiment, and the two different pathways are calculated to be similar in energy. This is likely due to the role of the additional aromatic rings in our model catalyst. The energy differences we calculate are quite small, suggesting that both of them may be involved in the reactions.

On the basis of these investigations, the “two-point binding models” of two different pathways shown in Figure 8 appear to

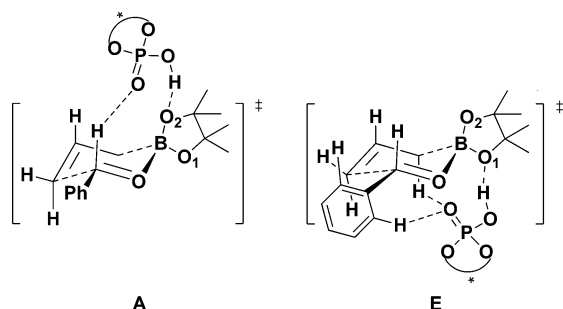


Figure 8. Models for the phosphoric acid catalyzed allylboration reaction.

operate for phosphoric acid catalyzed allylboration. The models consider two interactions between the catalyst and the substrates, which provide relative rigidity to the transition state. In what we will refer to as A (for axial), which is the same as Goodman’s model, the acidic H of the catalyst forms a hydrogen bond with the pseudoaxial oxygen of boronate. In E (for equatorial), the hydroxyl group of the catalyst H-bonds to the pseudoequatorial oxygen of boronate. The second interaction comes from the electrostatic attractions between the phosphoryl oxygen and relatively positive H’s.

Activation Barrier for Uncatalyzed and Catalyzed Reactions. Having investigated the mechanism and the model for this chiral phosphoric acid catalyzed allylboration reaction, the issue of the reactivity in the present reaction was then addressed. The uncatalyzed allylboration reaction between allylboration and benzaldehyde was studied first. The free energy profile is shown in Figure 9. A loose reactant complex C1 is formed with 7.9 free energy kcal/mol higher than the separated reactants. The activation free energy of the

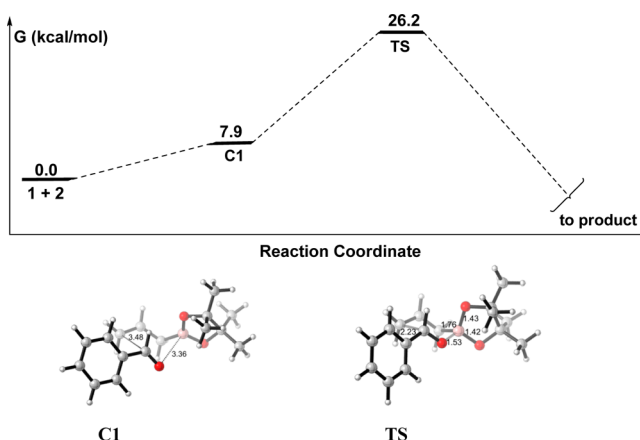


Figure 9. Reaction profile for the uncatalyzed allylboration reaction of 1 with 2 by B3LYP. Free energies relative the reactants in the gas phase. Optimized geometries of the complexes C1 and transition state TS are shown below the reaction profile.

uncatalyzed reaction relative to the separated reactants (1 + 2) was calculated to be high, 26.2 kcal/mol (Figure 9). This is consistent with the low reaction rates observed experimentally for the uncatalyzed allylboration reaction.¹⁷

For the phosphoric acid catalyzed reaction, in the E TS, the catalyst forms a hydrogen bond with the boronate pseudo-equatorial oxygen to afford complex C2 with free energy 0.6 kcal/mol higher than the separated reactants, as shown in Figure 10. The binding of benzaldehyde on C2 leads to the

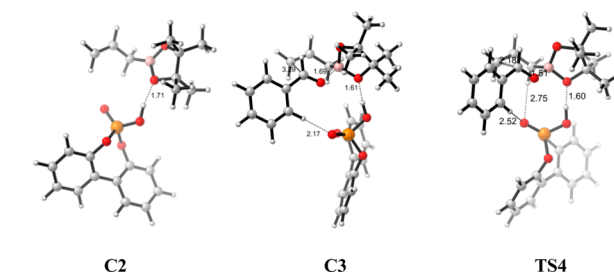
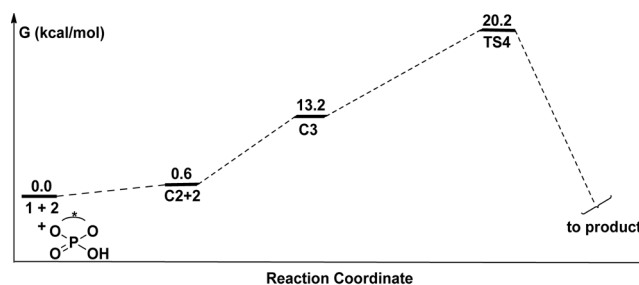


Figure 10. Reaction profiles for the allylboration reaction of 1 with 2 catalyzed by chiral phosphoric acid using E by B3LYP. Free energies relative the reactants in the gas phase. Optimized geometries of the complexes C2, C3 and transition state TS4 are shown below the reaction profile.

reactant complex C3. In transition state structure TS4, both the forming C–C and B–O bond distances (2.18 Å and 1.51 Å) are shorter than that in the uncatalyzed reaction TS (2.23 Å and 1.53 Å), which indicates the electrophilicity of boron is increased by catalyst activation. The calculated activation barrier of the catalyzed reaction relative to the separated reactants (1 + 2 + catalyst) is 20.2 kcal/mol (Figure 10), 6 kcal/mol lower than the uncatalyzed reaction.

On the other hand, for the A TS, the catalyst forms a hydrogen bond with the boronate pseudoaxial oxygen to afford complex C4, as shown in Figure 11. The binding of benzaldehyde on C4 leads to the reactant complex C5 with free energy 12.8 kcal/mol higher than the separated reactants. In TSS, the electrophilicity of boron is also increased by catalyst activation represented by the shorter C–C and B–O bond distances (2.14 Å and 1.50 Å) compared with that in the uncatalyzed reaction TS (2.23 Å and 1.53 Å), and the calculated activation barrier is 20.4 kcal/mol (Figure 11), 5.8 kcal/mol lower than the uncatalyzed reaction.

The two competing pathways give nearly identical energy profiles toward the catalyzed allylboration reactions, which again indicate the possibility that both two pathways are involved in the actual catalyzed reactions.

Origins of Enantioselectivity. The model studies described above indicated that both of the transition states in the two models, A and E, are likely to be involved in the reactions. To explore the origins of the enantioselectivity of the

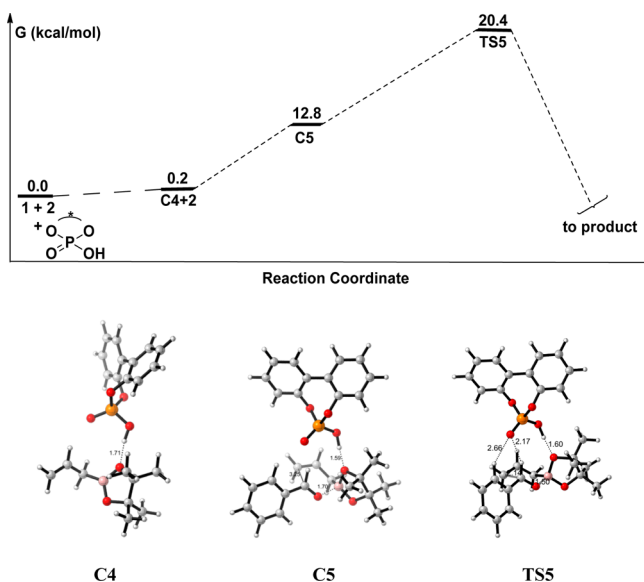


Figure 11. Reaction profiles for the allylboration reaction of **1** with **2** catalyzed by chiral phosphoric acid using **A** by B3LYP. Free energies relative the reactants in the gas phase. Optimized geometries of the complexes **C4**, **C5** and transition state **TS5** are shown below the reaction profile.

catalysis, the 3,3'-substituted BIPOL model for the binaphthol catalyst **PA1** was employed, and both transition states, **A** and **E**, were computed. Catalyst **PA1** bearing the 2,4,6-triisopropylphenyl group on the 3,3'-positions gave high enantioselectivity experimentally. The diastereomeric transition states for *re*-face (**r**) and *si*-face attack (**s**) involving BIPOL model of **PA1** were explored. The transition states involved were fully optimized, in contrast to Goodman's ONIOM calculations for these systems, **TSr1-E**, **TSs1-E** are located for **E** and **TSr1-A**, **TSs1-A** are located for **A**. These are shown in Figure 12.

In the equatorial coordination model **E**, the *re*-face attack **TSr1-E** is predicted to be more favored than the *si*-face attack **TSs1-E** by 2.0 kcal/mol. In the axial coordination model **A**, **TSr1-A** is more stable than **TSs1-A** by 6.1 kcal/mol using B3LYP calculations, which is consistent with Goodman's ONIOM calculations on these two TSs, which gives an energy difference of 6.7 kcal/mol.

In contrast to Goodman's ONIOM calculations that both *re* and *si* TSs are substantially energetically preferable in **A** over **E**, our fully optimized structure energies show that transition states resembling both models contribute to selectivity. That is, using the B3LYP-D3 energetics, the relative rates of reaction via **TSr1-A**, **TSr1-E**, and **TSs1-E** will be 1:0.05:0.001. Use of **A** only predicts far too high selectivity. The energy difference between the most stable *re*-face (**r**) attack transition state **TSr1-A** and the most stable *si*-face (**s**) attack transition state **TSs1-E** is 2.6 kcal/mol by B3LYP, which is in close agreement with the 93% ee observed experimentally. Solvation energy calculations using PCM model with toluene as the solvent does not change the energy difference very much, which gives a number of 3.1 kcal/mol.

On the basis of these calculations, we compare the two competing models for each enantiomeric TS (*re* or *si*), respectively. In Goodman's paper, the large preference for **A** comes from both steric and electronic factors. In the case of *re*-TSs, our calculations, in agreement with Goodman's results, show **A** (**TSr1-A**) is more stable than **E** (**TSr1-E**). Inspection

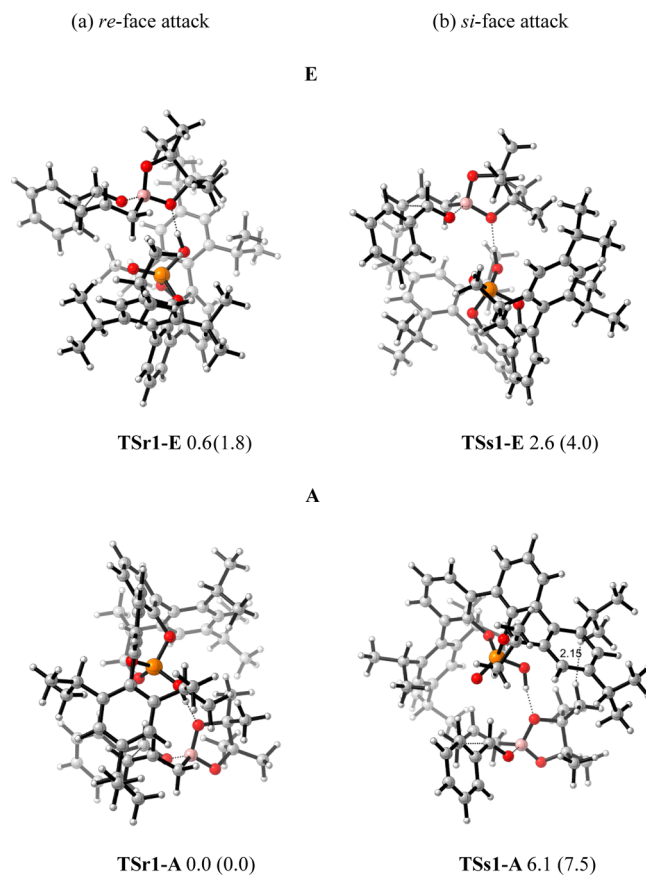


Figure 12. Optimized structures of **TSr1-E** and **TSs1-E** for **E** and **TSr1-A** and **TSs1-A** for **A**. Values next to each structure are energies relative to **TSr1-A** in kcal/mol. Values enclosed in parentheses are energies relative to **TSr1-A** calculated by B3LYP-D3.

of the two diastereomeric TSs show they are both free of steric problems by inspecting all of the H–H distances; all H–H distances are 2.4 Å or more. The stabilities between two TSs is then perhaps because formyl H-bond strength inside **A** (**TSr1-A**) is stronger than the electrostatic interactions between phosphoryl oxygen and relative positive H's in **E** (**TSr1-E**).

Our calculations show that **A** (**TSs1-A**) is much less favorable than **E** (**TSs1-E**) for *si*-TSs. In our fully optimized TS structures **TSs1-A** and **TSs1-E**, both of them have an almost linear H-bond arrangement. However, **A** (**TSs1-A**) has a longer H-bond distance (1.65 Å) and corresponding weaker H-bond strength than those in **E** (**TSs1-E**) (1.59 Å); this is opposite from Goodman's ONIOM calculated structures. We find a steric difference between the two models. Inspection of **A** (**TSs1-A**) shows that the pinacol group is orientated toward the bulky pocket of the catalyst, and there is one significant steric repulsion between an isopropyl H on the catalyst and a methyl H on the boronate, separated by only 2.15 Å; such steric repulsions are not found in **E** (**TSs1-E**). As a result, both electronic and steric factors make **A** (**TSs1-A**) less favorable than **E** (**TSs1-E**) in our calculated structures for *si*-TSs.

After comparing the two competing models, it is then necessary to investigate the origins of different stabilities between *re*- and *si*-TSs in each model, respectively. In **A**, the stabilities between **TSr1-A** and **TSs1-A** are due to steric factors. One significant steric repulsion between isopropyl H on the catalyst and methyl H on the boronate, separated by only 2.15 Å, was found for **TSs1-A**; by contrast **TSr1-A** is free of steric

congestion. These steric factors are believed to control the stabilities of two diastereomeric TSs in **A** in Goodman's studies as well.

In **E**, however, as mentioned above, there are no obvious steric differences in the two transition states **TSr1-E** and **TSs1-E**. To gain insights into the origins of the energy difference between **TSr1-E** and **TSs1-E**, the distortion energy (ΔE_d) and interaction energy (ΔE_i) of the transition states were performed. This method has been used previously to understand 1,3-dipolar and Diels–Alder cycloadditions.¹⁸ **TSr1-E** and **TSs1-E** are divided into two parts: catalyst-boronate complex **1A** and the benzaldehyde **1B** (Figure 13b) with the geometries fixed at the transition state geometries. The calculated distortion energy ΔE_d of **1B** in **TSr1-E** (+12.2 kcal/mol) is almost the same as that in **TSs1-E** (+12.3 kcal/mol). There is also no interaction energy ΔE_i difference between

TSr1-E (−41.3 kcal/mol) and **TSs1-E** (−41.2 kcal/mol), which means all of the stabilizing and destabilizing interactions between **1A** and **1B** in the two TSs are similar. The preference for *re*-facial selectivity is therefore the result of the larger distortion of catalyst-boronate complex **1A** in **TSs1-E**. **1A** is more heavily distorted in **TSs1-E** (+33.9 kcal/mol) than in **TSr1-E** (+32.1 kcal/mol) by 1.8 kcal/mol.

The origins of the differences in distortion energies of **1A** in the two TSs can be visualized from the **1A** geometries, as shown in Figure 13. In Figure 13d, which shows the **1A** structure in **TSs1-E**, the dioxaborolane ring is on the left, and the methyl groups on the dioxaborolane ring and isopropyl groups of catalysts are close to each other (green atoms in Figure 13d). In order to minimize such steric repulsions, the 2,4,6-triisopropylphenyl substituent is rotated around the bond to the BIPOL core with a dihedral angle of 80°. This is an 8° rotation away from the dihedral angle in the optimized catalyst (72°). Due to the distortion of the catalyst, the green atoms (Figure 13d) are all far away, resulting in no steric repulsions. In other words, the catalyst undergoes conformational changes to avoid unfavorable steric interactions in **TSs1-E**. Figure 13c shows the **1A** structure in **TSr1-E**. Here, the dioxaborolane ring is far from the catalyst, and the dihedral angle between 2,4,6-triisopropylphenyl substituent and the BIPOL core is 72°, the same as the dihedral angle of 72° in the optimized catalyst. The asymmetric induction can be rationalized by differences in distortion energies originating from avoiding the steric interactions between the substrates and the bulky 3,3'-substituents on the catalysts.

After investigating the allylboration reaction, we then reinvestigated the propargylations. The propargylation proceeds via a six-membered cyclic transition state similar to that for allylborations. Once again, the catalyst could activate the reaction by forming a hydrogen bond with either of the boronate oxygens. The transition state structures of propargylation involving the phosphoric acid catalyst **PAI** using both **E** and **A** were studied. As before, diastereomeric transition states **TSr1'-E** and **TSs1'-E** were located for **E**, and **TSr1'-A** and **TSs1'-A** were located for **A** (Figure 14).

As in the allylboration analysis, for *re*-face (**r**) attack, **A** (**TSr1'-A**) is more stable than **E** (**TSr1'-E**) by 2.7 (or 3.5) kcal/mol. For *si*-face (**s**) attack, **A** (**TSs1'-A**) is less stable than **E** (**TSs1'-E**) by 1.3 (or 1.2) kcal/mol. The energy difference between the most stable *re*-face (**r**) attack transition state **TSr1'-A** and the most stable *si*-face (**s**) attack transition state **TSs1'-E** is 4.0 (or 5.1) kcal/mol, overestimating the stereoselectivities as compared to the 74% ee observed experimentally.

Our studies on propargylations still showed that for *re*-TSs **A** is more favorable, while **E** is more favorable for *si*-TSs. The **A** and **E** transition states leading to *re* attack are both lower in energy than the **E** transition state that leads to *si* attack.

In **E**, the calculated distortion energy ΔE_d of benzaldehyde in **TSr1'-E** (+17.4 kcal/mol) is almost the same as that in **TSs1'-E** (+17.5 kcal/mol), so is the interaction energy ΔE_i for the two transition states. The preference for *re*-facial selectivity still comes from the larger distortion of catalyst-boronate complex in **TSs1'-E**. The catalyst-boronate complex is calculated to be more heavily distorted in **TSs1'-E** (+45.9 kcal/mol) than in **TSr1'-E** (+44.7 kcal/mol) by 1.2 kcal/mol.

The origin of the differences in distortion energies of catalyst-boronate complex in the two TSs is similar to that in the allylboration reaction. In Figure 15b, which shows the

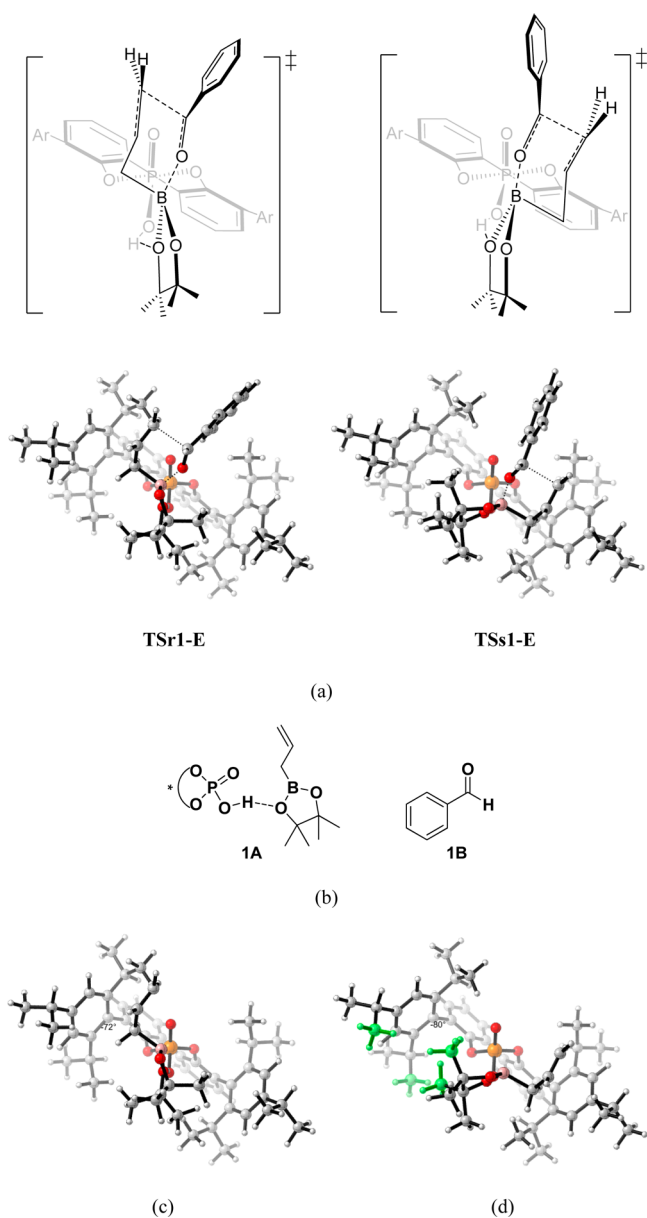


Figure 13. (a) Side view of **TSr1-E** and **TSs1-E**. (b) Structures of **1A** and **1B**. (c) 3D structures of **1A** in **TSr1-E**. (d) 3D structures of **1A** in **TSs1-E**.

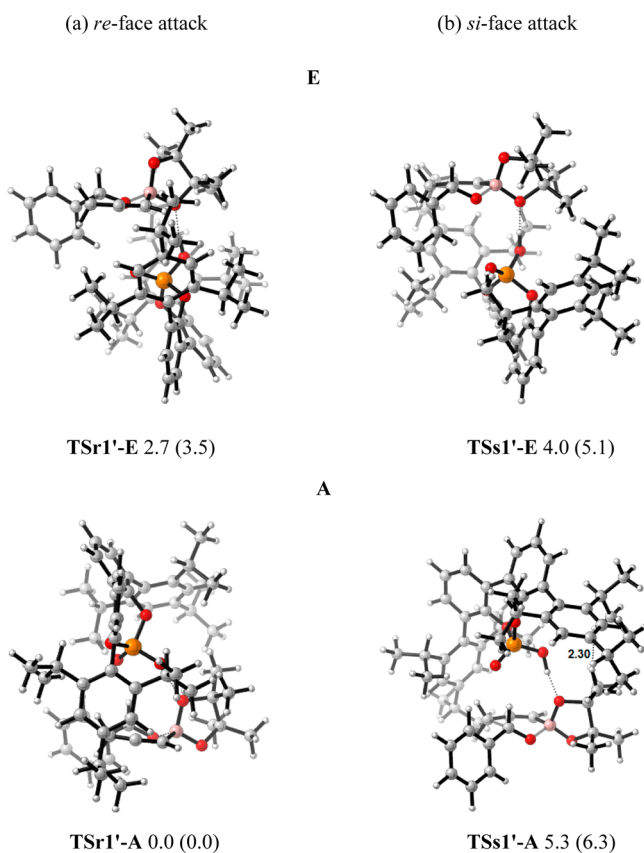


Figure 14. Optimized structures of TSr1'-E and TSs1'-E for E and TSr1'-A and TSs1'-A for A. Values next to each structure are energies relative to TSr1'-A in kcal/mol. Values enclosed in parentheses are energies relative to TSr1'-A calculated by B3LYP-D3.

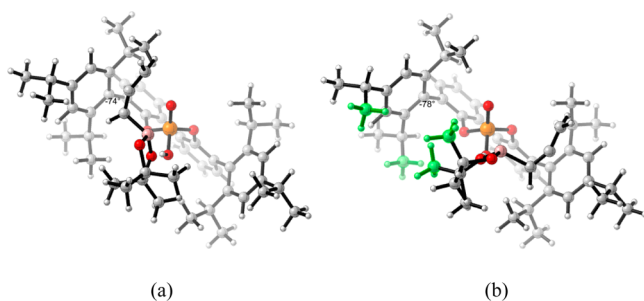


Figure 15. (a) 3D structure of TSr1'-E without the benzaldehyde. (b) 3D structure of TSs1'-E without the benzaldehyde.

complex structures in TSs1'-E, in order to minimize the steric repulsions between the methyl groups on the dioxaborolane ring and isopropyl groups of catalysts (green atoms in Figure 15b), the 2,4,6-triisopropylphenyl substituent is rotated around the bond to the BIPOL phenyl core with a dihedral angle of 78°. In Figure 15a, which shows the catalyst-boronate complex structure in TSr1'-E, the dihedral angle between 2,4,6-triisopropylphenyl substituent and the BIPOL core is 74°. The 4° dihedral angle differences of the two complexes accounts for their different distortion energies.

CONCLUSION

Theoretical calculations have been carried out for the chiral phosphoric acid catalyzed enantioselective allylboration and propargylation reactions. Transition states with either boronate

oxygen hydrogen-bonded to the phosphoric acid were studied. The catalyst is able to activate the boronate by forming a hydrogen bond either with the pseudo-equatorial oxygen (E) or the pseudoaxial oxygen (A) of the boronate; the phosphoryl oxygen interacts with relatively positive H's of the substrate through electrostatic attractions, which provides further stabilization of the TS, and a two-point orientation of the catalyst. Pathway A is investigated in detail in Goodman's model,⁹ and our studies focus more on pathway E in this paper.

For *re*-face attack, both equatorial and axial coordination gives TSs that are free of steric repulsions, with A more favorable than E. The relative stability of A is due to the formyl H-bond strength in A. For *si*-face attack, to give the minor enantiomer, our calculations showed that A is less favorable than E. Steric factors make the more crowded A less stable than the less crowded E.

Calculations show that the enantioselectivity observed experimentally originates from larger distortions of the catalyst in the minor enantiomeric TS, which is the result of the avoidance of the repulsive interactions between the bulky 3,3'-substituents in the catalyst and the substrates. The pinacol boronate methyls have an important role, and these groups could be altered to influence stereoselectivities. These investigations might help direct future enantioselective catalysis development for allylboration and propargylation reactions.

ASSOCIATED CONTENT

Supporting Information

Optimized geometries and energies of all computed species and full authorship of ref 12. This material is available free of charge via the Internet at <http://pubs.acs.org>.

AUTHOR INFORMATION

Corresponding Author

*E-mail: houk@chem.ucla.edu.

Notes

The authors declare no competing financial interest.

ACKNOWLEDGMENTS

This work was supported by the National Science Foundation (CHE 0614591) and National Institute of General Medical Sciences, National Institute of Health (GM36770). Computations were performed on the National Science Foundation Terascale Computing System at the National Center for Supercomputing Applications (NCSA), on the California NanoSystems Institute clusters and UCLA cluster.

REFERENCES

- (1) For reviews, see: (a) Denmark, S. E.; Almstead, N. G. In *Modern Carbonyl Chemistry*; Otera, J., Ed.; Wiley-VCH: Weinheim, 2000; Chapter 10, pp 299–402. (b) Chemler, S. R.; Roush, W. R. In *Modern Carbonyl Chemistry*; Otera, J., Ed.; Wiley-VCH: Weinheim, 2000; Chapter 11, 403–490. (c) Yamamoto, Y.; Asao, N. *Chem. Rev.* **1993**, *93*, 2207–2293. (d) Denmark, S. E.; Fu, J. *Chem. Rev.* **2003**, *103*, 2763–2793. (e) Lachance, H.; Hall, D. G. *Org. React.* **2008**, *73*, 1. (f) Roush, W. R. In *Comprehensive Organic Synthesis*; Trost, B. M., Ed.; Pergamon Press: Oxford, U.K., 1991; Vol. 2, p 1. (g) Yus, M.; González-Gómez, J. C.; Foubelo, F. *Chem. Rev.* **2011**, *111*, 7774–7854.
- (2) (a) Roush, W. R.; Walts, A. E.; Hoong, L. K. *J. Am. Chem. Soc.* **1985**, *107*, 8186–8190. (b) Roush, W. R.; Palkowitz, A. D.; Ando, K. *J. Am. Chem. Soc.* **1990**, *112*, 6348–6359. (c) Brown, H. C.; Bhat, K. S.; Randad, R. S. *J. Org. Chem.* **1989**, *54*, 1570–1576. (d) Brown, H. C.; Randad, R. S.; Bhat, K. S.; Zaidlewicz, M.; Racherla, U. S. *J. Am. Chem. Soc.* **1990**, *112*, 2389–2392. (e) Corey, E. J.; Yu, C.-M.; Lee, D.-H. *J.*

- Am. Chem. Soc.* **1990**, *112*, 878–879. (f) Gonzalez, A. Z.; Roman, I. G.; Alicea, E.; Canales, E.; Soderquist, J. A. *J. Am. Chem. Soc.* **2009**, *131*, 1269–1273. (g) Burgos, C. H.; Canales, E.; Matos, K.; Soderquist, J. A. *J. Am. Chem. Soc.* **2005**, *127*, 8044–8049. (h) Wu, T. R.; Shen, L.; Chong, J. M. *Org. Lett.* **2004**, *6*, 2701–2704. (i) Lachance, H.; Lu, X.; Gravel, M.; Hall, D. G. *J. Am. Chem. Soc.* **2003**, *125*, 10160–10161. (j) Chen, M.; Handa, M.; Roush, W. R. *J. Am. Chem. Soc.* **2009**, *131*, 14602–14603. (k) Althaus, M.; Mahmood, A.; Suarez, J. R.; Thomas, S. P.; Aggarwal, V. K. *J. Am. Chem. Soc.* **2010**, *132*, 4025–4028.
- (3) (a) Kennedy, J. W. J.; Hall, D. G. *J. Am. Chem. Soc.* **2002**, *124*, 11586–11587. (b) Lachance, H.; Xu, M.; Gravel, M.; Hall, D. G. *J. Am. Chem. Soc.* **2003**, *125*, 10160–10161. (c) Hall, D. G. *Synlett* **2007**, 1644–1655. (d) Kennedy, J. W. J.; Hall, D. G. *J. Org. Chem.* **2004**, *69*, 4412–4428. (e) Rauniyar, V.; Hall, D. G. *J. Am. Chem. Soc.* **2004**, *126*, 4518–4519. (f) Carosi, L.; Lachance, H.; Hall, D. G. *Tetrahedron* **2005**, *46*, 8981–8985. (g) Rauniyar, V.; Zhai, H.; Hall, D. G. *J. Am. Chem. Soc.* **2008**, *130*, 8481–8490. (h) Rauniyar, V.; Hall, D. G. *J. Org. Chem.* **2009**, *74*, 4236–4241. (i) Ishiyama, T.; Ahiko, T.-a.; Miyaura, N. *J. Am. Chem. Soc.* **2002**, *124*, 12414–12415. (j) Wada, R.; Oisaki, K.; Kanai, M.; Shibasaki, M. *J. Am. Chem. Soc.* **2004**, *126*, 8910–8911.
- (4) (a) Yu, S. H.; Ferguson, M. J.; McDonald, R.; Hall, D. G. *J. Am. Chem. Soc.* **2005**, *127*, 12808–12809. (b) Rauniyar, V.; Hall, D. G. *Angew. Chem., Int. Ed.* **2006**, *45*, 2426–2428. (c) Elford, T. G.; Arimura, Y.; Yu, S. H.; Hall, D. G. *J. Org. Chem.* **2007**, *72*, 1276–1284. (d) Rauniyar, V.; Zhai, H.; Hall, D. G. *J. Am. Chem. Soc.* **2008**, *130*, 8481–8490.
- (5) For reviews, see: (a) Akiyama, T. *Chem. Rev.* **2007**, *107*, 5744–5758. (b) Terada, M. *Chem. Commun.* **2008**, 4097–4112. (c) Brunel, J. M. *Chem. Rev.* **2005**, *105*, 857–897. (d) Chen, Y.; Yekta, S.; Yudin, A. K. *Chem. Rev.* **2003**, *103*, 3155–3211. (e) Akiyama, T.; Itoh, J.; Fuchibe, K. *Adv. Synth. Catal.* **2006**, *348*, 999–1010. (f) Connors, S. J. *Angew. Chem., Int. Ed.* **2006**, *45*, 3909–3912. (g) Rueping, M.; Kuenkel, A.; Atodiresei, I. *Chem. Soc. Rev.* **2011**, *40*, 4539–4549. (h) Zamfir, A.; Schenker, S.; Freund, M.; Tsogoeva, S. B. *Org. Biomol. Chem.* **2010**, *8*, 5262–5276.
- (6) For theoretical studies on the chiral phosphoric acid catalysis, see: (a) Yamanaka, M.; Itoh, J.; Fuchibe, K.; Akiyama, T. *J. Am. Chem. Soc.* **2007**, *129*, 6756–6764. (b) Simón, L.; Goodman, J. M. *J. Am. Chem. Soc.* **2008**, *130*, 8741–8747. (c) Simón, L.; Goodman, J. M. *J. Am. Chem. Soc.* **2009**, *131*, 4070–4077. (d) Simón, L.; Goodman, J. M. *J. Org. Chem.* **2010**, *75*, 589–597. (e) Simón, L.; Goodman, J. M. *J. Org. Chem.* **2011**, *76*, 1775–1788. (f) Marcelli, T.; Hammar, P.; Himo, F. *Chem.—Eur. J.* **2008**, *14*, 8562–8571. (g) Akiyama, T.; Morita, H.; Bachu, P.; Mori, K.; Yamanaka, M.; Hirata, T. *Tetrahedron* **2009**, *65*, 4950–4956. (h) Shi, F.-Q.; Song, B.-A. *Org. Biomol. Chem.* **2009**, *7*, 1292–1298. (i) Yamanaka, M.; Hirata, T. *J. Org. Chem.* **2009**, *74*, 3266–3271. (j) Gridnev, I. D.; Kouchi, M.; Sorimachi, K.; Terada, M. *Tetrahedron Lett.* **2007**, *48*, 497–500.
- (7) Jain, P.; Antilla, J. C. *J. Am. Chem. Soc.* **2010**, *132*, 11884–11886.
- (8) Jain, P.; Wang, H.; Houk, K. N.; Antilla, J. C. *Angew. Chem., Int. Ed.* **2012**, *124*, 1420–1423.
- (9) Grayson, M. N.; Pellegrinet, S. C.; Goodman, J. M. *J. Am. Chem. Soc.* **2012**, *134*, 2716–2722.
- (10) (a) For dispersion correction, see: (a) Grimme, S. *J. Comput. Chem.* **2006**, *27*, 1787–1799. (b) Grimme, S.; Antony, J.; Ehrlich, S.; Krieg, H. *J. Chem. Phys.* **2010**, *132*, 154104. For application of dispersion corrected DFT in computational chemistry, see: (c) McMullin, C. L.; Jover, J.; Harvey, J. N.; Fey, N. *Dalton Trans.* **2010**, 39, 10833–10836. (d) Antoline, J. E.; Krenske, E. H.; Lohse, A. G.; Houk, K. N.; Hsung, R. P. *J. Am. Chem. Soc.* **2011**, *133*, 14443–14451.
- (11) (a) Li, Y.; Houk, K. N. *J. Am. Chem. Soc.* **1989**, *111*, 1236–1240. (b) Gung, B. W.; Xue, X.; Roush, W. R. *J. Am. Chem. Soc.* **2002**, *124*, 10692–10697.
- (12) Frisch, M. J. et al. *Gaussian 09*, revision B.01; Gaussian, Inc.: Wallingford, CT, 2010.
- (13) (a) Omoto, K.; Fujimoto, H. *J. Org. Chem.* **1998**, *63*, 8331–8336. (b) Brown, H. C.; Racherla, U. S.; Pellechia, P. J. *J. Org. Chem.* **1990**, *55*, 1868–1874.
- (14) Rauniyar, V.; Hall, D. G. *J. Am. Chem. Soc.* **2004**, *126*, 4518–4519.
- (15) Sakata, K.; Fujimoto, H. *J. Am. Chem. Soc.* **2008**, *130*, 12519–12526.
- (16) (a) Corey, E. J.; Rohde, J. J.; Fischer, A.; Azimioara, M. D. *Tetrahedron Lett.* **1997**, *38*, 33–36. (b) Corey, E. J.; Rohde, J. J. *Tetrahedron Lett.* **1997**, *38*, 37–40. (c) Corey, E. J.; David, B. S.; Thomas, W. L. *Tetrahedron Lett.* **1997**, *38*, 1699–1702.
- (17) Ishiyama, T.; Ahiko, T.; Miyaura, N. *J. Am. Chem. Soc.* **2002**, *124*, 12414–12415.
- (18) (a) Ess, D. H.; Houk, K. N. *J. Am. Chem. Soc.* **2008**, *130*, 10187–10198. (b) Ess, D. H.; Houk, K. N. *J. Am. Chem. Soc.* **2007**, *129*, 10646–10647. (c) Ess, D. H.; Jones, G. O.; Houk, K. N. *Org. Lett.* **2008**, *10*, 1633–1636. (d) García, J. I.; Martínez-Merino, V.; Mayoral, J. A.; Salvatella, L. *J. Am. Chem. Soc.* **1998**, *120*, 2415–2420. (e) Sbai, A.; Branchadell, V.; Ortuño, R. M.; Oliva, A. *J. Org. Chem.* **1997**, *62*, 3049–3054.